Letter

Topological superconductivity in $LaFe_2As_2$ and $LaBaFe_4As_4$ studied by DFT+DMFT first-principles calculations

Pengyu Zheng,[1] Guangwei Wang,[1] Rui Liu,[1] Zhihong Yuan,[1] Yiran Peng,[1] Tianye Yu,[1] and Zhiping Yin[1,2,*]

[1]*School of Physics & Astronomy and Center for Advanced Quantum Studies, Beijing Normal University, Beijing 100875, China*
[2]*Key Laboratory of Multiscale Spin Physics (Ministry of Education), Beijing Normal University, Beijing 100875, China*

We investigate the electronic structure and topological properties of iron-based superconductors $LaFe_2As_2$ using density functional theory plus dynamical mean-field theory. We find that the uncollapsed tetragonal $LaFe_2As_2$ is in a nontrivial Z_2 topological phase and has topological Dirac surface states near the Fermi energy which suggests there could be Majorana zero modes in the superconducting $LaFe_2As_2$. In light of the nontrivial topological properties and superconductivity of $LaFe_2As_2$ and $CaKFe_4As_4$, we predict a new iron-based compound $LaBaFe_4As_4$ and find it possesses two sets of topological Dirac surface states near the Fermi energy despite of a trivial Z_2 topological index. These topological surface states are induced by a nontrivial high-order topological index Z_8, a new mechanism that is distinct from all-known iron-based superconductors. Our study not only demonstrates that both $LaBaFe_4As_4$ and uncollapsed tetragonal $LaFe_2As_2$ can be good platforms for exploring topological superconductivity but also paves a new way to realize it with a nontrivial high-order topological index.

Iron-based superconductors [1–12] have attracted new research interests in recent years due to the observation of topological surface states and Majorana zero modes in some of them [13–20]. For examples, topological Dirac surface states and Majorana zero modes (MZMs) were found in Fe(Se,Te), (Li,Fe)OHFeSe, and $CaKFe_4As_4$ [21–24]. Li(Fe,Co)As was found to possess both topological insulator (TI) surface states and topological Dirac semimetal (TDS) surface states [25]. The coexistence of topological surface states and superconductivity in these iron-based superconductors make them good platforms for studying surface topological superconductivity [24,26,27] and bulk topological superconductivity [28–30]. It is interesting to look for more iron-based superconductors which can serve as good platforms for exploring topological superconductivity and MZMs.

In 2019, Akira Iyo *et al.* successfully synthesized both uncollapsed tetragonal (UT) and collapsed tetragonal (CT) $LaFe_2As_2$ (UT-LFA and CT-LFA). They found superconductivity in UT-LFA with $T_c \sim 12.1$ K but not in CT-LFA [31]. Several groups have reported the correlation strength [32–34] and electronic structures of $LaFe_2As_2$, featuring the absence of hole Fermi surfaces (FS) around Γ point [34–37]. However, the topological properties of $LaFe_2As_2$ are still unknown. If UT-LFA has nontrivial band topology and topological surface states, it can also harbor MZMs on its surface.

Doping is a common way to fine tune the electronic structures and other properties of materials. 50% doping at the alkaline earth metal site of a 122-type iron-based superconductor (e.g., $CaFe_2As_2$) can result in a new 1144-type iron-based superconductor (e.g. $CaKFe_4As_4$) [38–42]. The 1144-type iron-based superconductors possess high T_c around 30 K [43] and have received lots of attention on their special magnetism [41,44,45] and topological states [46]. Even more interesting, using angle-resolved photoemission spectroscopy and scanning tunneling microscopy/spectroscopy measurement as well as electronic structure calculations, Wenyao Liu *et al.* found topological Dirac surface states and MZMs in $CaKFe_4As_4$ [23]. This finding inspires us to design a new 1144-type iron-based superconductor which has both high-T_c and topological surface states.

In this paper, we carry out density functional theory plus dynamical mean-field theory (DFT+DMFT) calculations of the electronic structures and topological properties of $LaFe_2As_2$ and the newly designed $LaBaFe_4As_4$. We find that the superconducting uncollapsed tetragonal $LaFe_2As_2$ is in a nontrivial topological phase and has topological Dirac surface states near the Fermi energy on the (001) surface, which suggests that Majorana zero modes could emerge on its (001) surface. We further design a new 1144-type $LaBaFe_4As_4$ compound and find that it has both the topological insulator surface states and topological Dirac semimetal surface states near the Fermi energy on the (001) surface, similar to the aforementioned Li(Fe,Co)As. Moreover, we find that, due to the unique electronic structure of $LaBaFe_4As_4$, the double topological insulator surface states emerge from a nontrivial high-order topological index Z_8, instead of a trivial strong topological index ν_0 of Z_2, which is very rare. Our study not only indicates that both the uncollapsed tetragonal $LaFe_2As_2$ and the newly designed $LaBaFe_4As_4$ can be good platforms for exploring topological superconductivity, but also provides a new mechanism to realize them using nontrivial high-order topological index.

We first discuss the electronic structure and topological property of UT-LFA. As shown in Fig. S1(a) in Ref. [47] (see
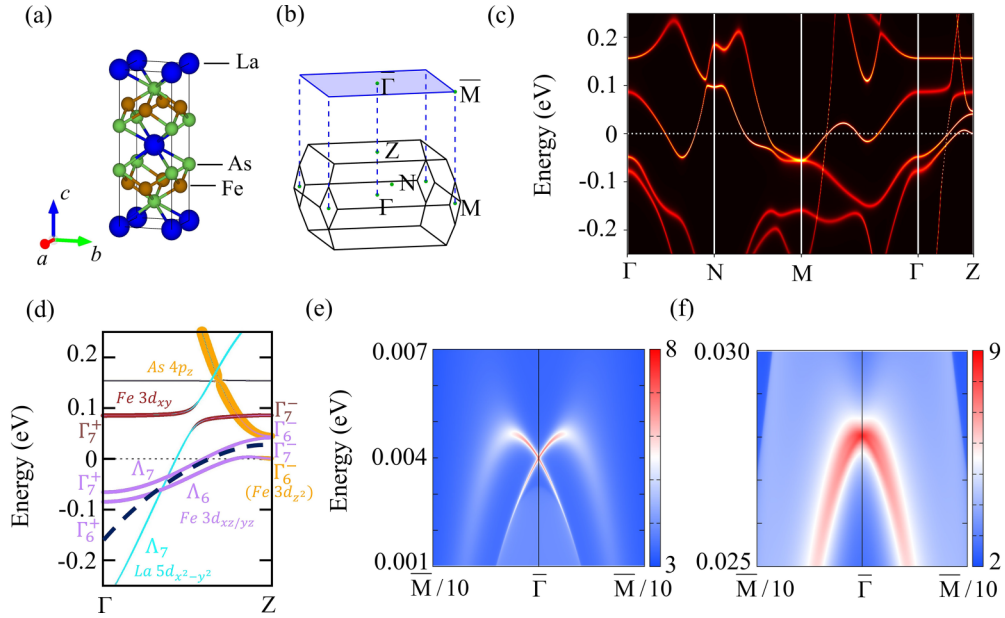

FIG. 1. The crystal structure (a), three-dimensional Brillouin zone (BZ) and projected (001) surface BZ (b), DFT+DMFT band structure with SOC (c), band topology along Γ-Z (d) and surface states [(e) and (f)] based on the DFT+DMFT tight-binding (TB) model of uncollapsed tetragonal LaFe$_2$As$_2$. (d) The fatbands and irreducible representations along Γ-Z based on the DFT+DMFT TB model, where the black dashed line represents the Fermi curve, the orange, brown, purple, and cyan colors represent the As-4p_z, Fe-3d_{xy}, Fe-3$d_{xz/yz}$, and La-5$d_{x^2-y^2}$ orbital characters, respectively. In order to highlight the hybridization between the As-4p_z-dominated band and Fe-3$d_{xz/yz}$-dominated band, we enlarge the orange solid circles by a factor of 3 compared to the others. [(e) and (f)] The surface states on the As-terminated (001) surface (e) and La-terminated (001) surface (f) based on the DFT+DMFT TB model.

also Refs. [48–74] therein), our DFT+DMFT band structure without considering spin-orbit coupling (SOC) is consistent with Ref. [34]. Here we focus on the band structure with SOC and the topological property which has not been reported previously. There are two equivalent time-reversal invariant points (TRIPs) M points and four equivalent N points in the Brillouin zone (BZ) of UT-LFA [Fig. 1(b)]. These six points yield a trivial parity product. Based on the Fu-Kane criterion on the Z_2 invariant of materials with inversion symmetry [63], we only need to know the band inversions and parity changes between Γ and Z points to determine its strong topological index of Z_2, i.e., ν_0. For this purpose, a Fermi curve is defined for the topological index of interest, and its energy (the nominal "Fermi energy") becomes momentum-dependent for metals [21] (see details in Ref. [47]).

Compared to the DFT band structure [Fig. S1(b)] [47], besides an overall compression of the band width, we find that after considering electronic correlation effects, the As-4p_z orbital dominated band with a negative slope hybridizes with the Fe-3$d_{xz/yz}$ orbital dominated bands along the Γ-Z direction very close to the Z point and E_F, opening a hybridization gap [Figs. 1(c) and 1(d)]. This hybridization has no effect on the parity product of Γ and Z points compared to the DFT results because both bands have Γ_6^- symmetry/parity at Z point (the lower Γ_6^- state near E_F at Z point should be attributed to Fe-3d_{z^2} orbital as shown in Fig. 1(d) and Fig. S2 [47]). However, it changes the nature of the band inversion which happens between the As-4p_z and the Fe-3d_{z^2} orbital dominated bands in DFT whereas it happens between the As-4p_z and the Fe-3$d_{xz/yz}$ orbital dominated bands in DFT+DMFT (see details in Ref. [47]).

The Fermi curve in Fig. 1(d) is not well defined because it will cross a Dirac point protected by the crystal C_{4v} symmetry (the crossing between the purple Λ_6 and cyan Λ_7 bands). However, once the C_{4v} symmetry is lifted by a small pertubation, the Fermi curve becomes well defined and results in a strong topological index $\nu_0 = 1$ for all the bands below this Fermi curve. This feature of the band structure makes bulk three-dimensional (3D) Dirac points and $\nu_0 = 1$ coexist in UT-LFA, similar to the cases of Na$_3$Bi [75] and β-CuI [76]. Differing from Na$_3$Bi, the 3D Dirac points in UT-LFA belong to the type-II and are buried in the bulk states on the (001) surface. The nontrivial strong topological index $\nu_0 = 1$ gives rise to Dirac-cone type topological surface states on the (001) surface as shown in Figs. 1(e) and 1(f). By comparing the Dirac-cone type topological surface states in Figs. 1(e) and S1(d) [47], we notice that electronic correlation moves the topological surface states much closer to E_F as discussed in Ref. [14], which is good for realizing topological superconducting states.

In light of the coexistence of superconductivity and nontrivial topological properties in CaKFe$_4$As$_4$ [23] and UT-LFA, we design a new iron-based superconductor LaBaFe$_4$As$_4$. Based on the work of Akira Iyo *et al.* [43], AeAFe$_4$As$_4$ (Ae= Ca, Sr; A= K, Rb, Cs) is formed as a line phase, so we can infer the lattice parameters of LaBaFe$_4$As$_4$ by averaging the experimental values of LaFe$_2$As$_2$ [31] and BaFe$_2$As$_2$ [77]. More results and details of the optimization of the internal atomic coordinates and dynamical stabilities of the newly designed LaBaFe$_4$As$_4$ are presented in Ref. [47].

Figure 2 shows the crystal structure, BZ, DFT+DMFT density of states (DOS) and band structure of LaBaFe$_4$As$_4$.
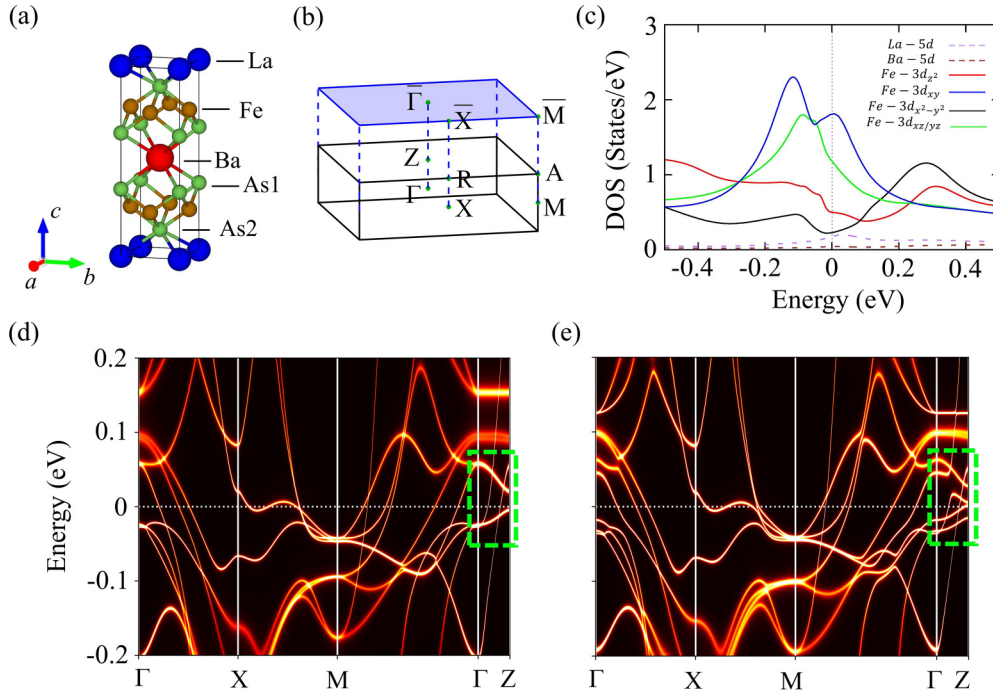
FIG. 2. The crystal structure (a), three-dimensional BZ and projected (001) surface BZ (b), DFT+DMFT density of states (c), and band structures without SOC (d) and with SOC (e) of LaBaFe$_4$As$_4$. The green dashed boxes in (d) and (e) highlight the band crossing and anticrossing of interest.

The 50% substitution of La with Ba breaks the glide symmetry of the 122 structure [Figs. 1(a) and 2(a)] and results in the doubling of the unit cell along c axis. Consequently, the number of bands doubles and there are more FS sheets compared to 122-type iron-based compounds. Unlike CaKFe$_4$As$_4$ [42], a La-5$d_{x^2-y^2}$ orbital dominated band, appears around E_F in the band structure of LaBaFe$_4$As$_4$ [Figs. 3(a) and S4(f)] [47] and influences the subsequent analysis of its topological property. Without SOC, we observe several band crossings along Γ-Z in the energy range from -0.2 to 0.2 eV, including crossings between the La-5$d_{x^2-y^2}$ orbital dominated band and the Fe-3$d_{xz/yz}$ orbital dominated band, the As-4p_z orbital dominated band and the Fe-3$d_{xz/yz}$, $3d_{xy}$, $3d_{x^2-y^2}$ orbitals dominated bands [Fig. 2(d), Fig. S4 and S5(c)] [47]. With SOC, the degenerate Fe-3$d_{xz/yz}$ orbital dominated band split into two bands and hybridization gaps are opened at some crossing points [Fig. 2(e) and 3(a)].

Similar to other iron-based compounds, we find the Fe-3$d_{t_{2g}}$ orbitals contribute much more than the Fe-3d_{e_g} orbitals around E_F [Fig. 2(c)], which is also reflected in the orbital-resolved FS [Figs. S5(d) and S5(e)] [47]. The contribution of La-5d orbitals can also be seen around E_F whereas the Ba-5d orbitals have negligible DOS around E_F.

Compared to other 1144-type iron-based superconductors like CaKFe$_4$As$_4$ [42], LaBaFe$_4$As$_4$ has similar band structure and FS, especially the nearly ideal nesting between the hole-like FS around Γ and the electron-like FS around M [Figs. S5(a) and S5(d)] [47], which enhances Cooper pairing and makes the superconducting gaps larger in CaKFe$_4$As$_4$ [38]. We also notice that even with large magnetic moments on Eu sites, RbEuFe$_4$As$_4$ still possesses high T_c equal to 35 K [41] which to some extent supports the robustness of

superconductivity of 1144-type iron-based compounds. Based on the above facts, we believe LaBaFe$_4$As$_4$ has a good chance to superconduct with a high T_c.

We now turn to the topological property of LaBaFe$_4$As$_4$. Unlike UT-LFA, four TRIPs Γ, Z, M, and A are needed to determine ν_0 (two equivalent X points and R points yield a trivial parity product). In Figs. 3(a) and 3(e), we draw two possible Fermi curves and calculate ν_0 for all the bands below them.

For the Fermi curve indicated by the black dashed line, there are two band inversions along Γ-Z around the Fermi curve: one occurs between the As1-4p_z orbital dominated band (Γ_6^+) and the Fe-3$d_{xz/yz}$ orbital dominated band (Γ_6^-), and the other occurs between the La-5$d_{x^2-y^2}$ orbital dominated band (Γ_7^+) and the Fe-3$d_{xz/yz}$ orbital dominated band (Γ_7^-). Each band inversion brings a -1 product of the parity at Γ and Z points of the corresponding bands below the Fermi curve. However, two such band inversions contribute a $+1$ parity product of all the bands at Γ and Z points below this Fermi curve. Detailed analysis of the bands along M-A path also gives rise to a parity product of $+1$ for all the bands below this Fermi curve at M and A points [47]. Therefore the strong topological index ν_0 equals to 0 for all the bands below the Fermi curve defined by the black-dashed line in Fig. 3(a).

Interestingly, as shown in Fig. 3(b), we find that the aforementioned two band inversions occurring along the Γ-Z path, while contributing a trivial parity product together, bring two sets of TI surface states around the BZ center on the (001) surface. These TI surface states are robust as long as the gaps and band inversions exist, differing from the fragile Dirac-cone type surface states at multiple (even number) TRIPs in the surface BZ of a weak TI with $\nu_0 = 0$ [63,67].
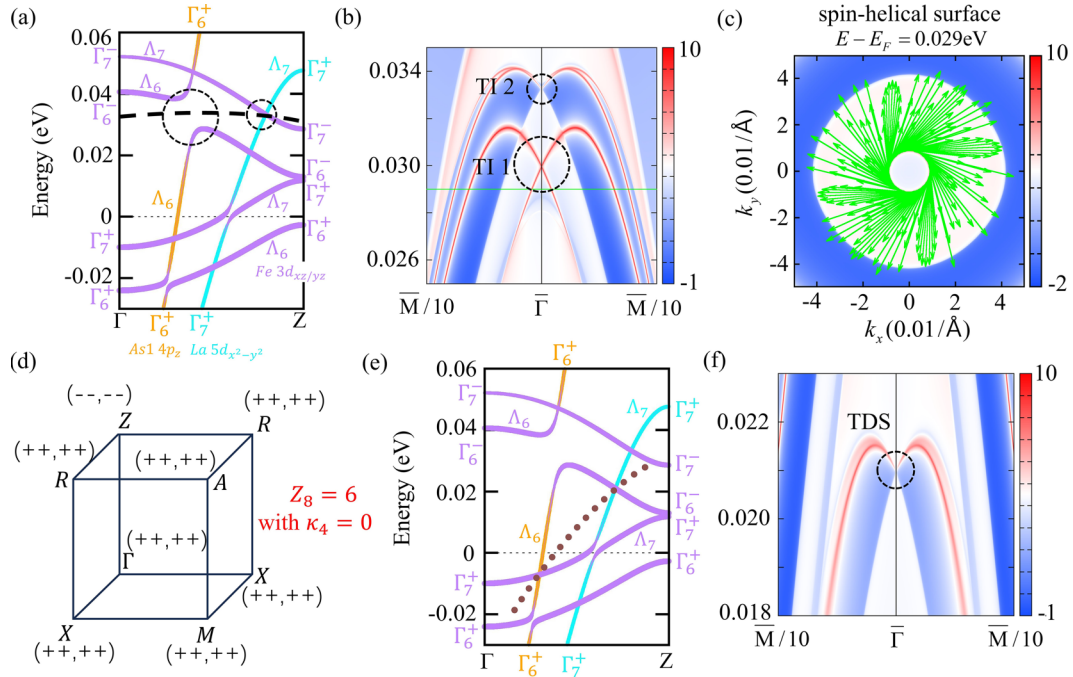
FIG. 3. The DFT+DMFT band topology, surface states and spin textures of LaBaFe$_4$As$_4$. [(a) and (e)] The DFT+DMFT TB model based fatbands and irreducible representation along Γ-Z. The black dashed (a) and brown dotted (d) lines represent two different choices of the Fermi curve. The orange, purple, and cyan colors represent the As1-4p_z, Fe-3$d_{xz/yz}$, and La-5$d_{x^2-y^2}$ orbital characters, respectively. [(b) and (f)] The surface states on the As1-terminated (001) surface based on the DFT+DMFT TB model, in which the TI and TDS represent topological insulator states and topological Dirac semimetal states, respectively. (c) The two-dimensional constant-energy surface states on the As1-terminated (001) surface. The constant energy (29 meV) is marked by a green solid line in (b). The spin textures are indicated by green arrows. (d) Schematic diagram of the nontrivial high-order topological index of double topological insulator (TI) states.

The emergence of two sets of TI surface states from a trivial topological index Z_2 is very unusual, and have not been reported in iron-based superconductors to our best knowledge. It is very important to understand why and how these TI surface states emerge. After extensive research and verification, we find that we can use the high-order topological index Z_8 to characterize these double TI states [69,74,78], based on the following formula [69]:

$$Z_8 = \kappa_1 - 2\kappa_4 \text{ mod } 8 \tag{1}$$

in which K is a TRIP, $\kappa_1 = \frac{1}{4}\sum_{K \in \text{TRIPs}}(n_K^+ - n_K^-)$, n_K^+ (n_K^-) is the number of bands with even (odd) parity at K, and $\kappa_4 = \frac{1}{2\sqrt{2}}\sum_{K \in K_4}\sum_\alpha e^{i(\alpha\pi/4)}n_K^\alpha$, where n_K^α is the number of bands with the eigenvalue $e^{i(\alpha\pi/4)}$ at K ($\alpha = 1$, 3, 5, or 7) and K_4 are those TRIPs that are invariant under S_4 symmetry operation. Specifically, K_4 are the following TRIPs: (0,0,0), (0.5,0.5,0), (0,0,0.5), and (0.5,0.5,0.5) in the units of the reciprocal lattice vectors of the primitive cell. We can now simplify the DFT+DMFT band topology of LBFA as a four-band case. Since κ_4 is equal to 0 in our case [47], we only show the parities of the bands at TRIPs in Fig. 3(d) in order to calculate the Z_8 index, which turns out to be 6, thus confirming the topologically nontrivial properties of LBFA.

We also check the spin-texture at a constant energy 29 meV below the Dirac point of the lower TI surface states shown in Fig. 3(b) by a green line. A spin-helical surface state is

found which forms a π Berry phase enclosed [Fig. 3(c)] and confirms the nontrival topological nature of the bulk band structure of LBFA. Therefore it is very interesting to investigate LaBaFe$_4$As$_4$ experimentally for both proving the nontrivial high-order topological index induced topological surface states in iron-based compounds and looking for a new platfrom harboring topological superconductivity.

For the Fermi curve indicated by the brown dotted line shown in Fig. 3(e), only one band inversion between the La-5$d_{x^2-y^2}$ orbital dominated band (Γ_7^+) and the Fe-3$d_{xz/yz}$ orbital dominated band (Γ_6^-) occurs. The Fermi curve passes through two Dirac points along Γ-Z which are protected by the crystal C_{4v} symmetry. These give rise to TDS surface states on the (001) surface as shown in Fig. 3(f), similar to the TDS surface states reported in Li(Fe,Co)As [25].

In conclusion, we investigate the topological property of UT-LFA and find that the superconducting UT-LFA is in a nontrivial topological phase and has topological Dirac surface states near E_F on the (001) surface, which suggests that MZMs have a good chance to emerge on its (001) surface. We further predict a candidate iron-based superconductor LaBaFe$_4$As$_4$ with multiple topological surface states on the (001) surface near E_F which suggests it can harbors topological superconductivity. Surprisingly, two sets of topological Dirac surface states on the (001) surface emerge from a nontrivial Z_8 topological index, despite a trivial Z_2 topological index. Our findings not only call for experimental verifications but also unveil a new way to realize topological Dirac

surface states *via* a nontrival high-order topological index. Our work suggests both UT-LFA and LaBaFe$_4$As$_4$ are good platforms for exploring topological superconductivity. It is also interesting to explore other rare earth-related iron-based compounds to realize 5d-orbital related novel band topology and topological surface states from a nontrival high-order topological index.

[1] G. R. Stewart, Superconductivity in iron compounds, Rev. Mod. Phys. **83**, 1589 (2011).

[2] D. J. Scalapino, A common thread: The pairing interaction for unconventional superconductors, Rev. Mod. Phys. **84**, 1383 (2012).

[3] P. Dai, Antiferromagnetic order and spin dynamics in iron-based superconductors, Rev. Mod. Phys. **87**, 855 (2015).

[4] P. Dai, J. Hu, and E. Dagotto, Magnetism and its microscopic origin in iron-based high-temperature superconductors, Nat. Phys. **8**, 709 (2012).

[5] X. Chen, P. Dai, D. Feng, T. Xiang, and F.-C. Zhang, Iron-based high transition temperature superconductors, Natl. Sci. Rev. **1**, 371 (2014).

[6] Y. Kamihara, T. Watanabe, M. Hirano, and H. Hosono, Iron-based layered superconductor La[O$_{1-x}$F$_x$]FeAs (x = 0.05-0.12) with T$_c$ = 26 K, J. Am. Chem. Soc. **130**, 3296 (2008).

[7] J. Paglione and R. L. Greene, High-temperature superconductivity in iron-based materials, Nat. Phys. **6**, 645 (2010).

[8] M. Rotter, M. Tegel, and D. Johrendt, Superconductivity at 38 K in the iron arsenide (Ba$_{1-x}$K$_x$)Fe$_2$As$_2$, Phys. Rev. Lett. **101**, 107006 (2008).

[9] X. F. Lu, N. Z. Wang, H. Wu, Y. P. Wu, D. Zhao, X. Z. Zeng, X. G. Luo, T. Wu, W. Bao, G. H. Zhang, F. Q. Huang, Q. Z. Huang, and X. H. Chen, Coexistence of superconductivity and antiferromagnetism in (Li$_{0.8}$Fe$_{0.2}$)OHFeSe, Nat. Mater. **14**, 325 (2015).

[10] Z. P. Yin, K. Haule, and G. Kotliar, Magnetism and charge dynamics in iron pnictides, Nat. Phys. **7**, 294 (2011).

[11] Z. P. Yin, K. Haule, and G. Kotliar, Kinetic frustration and the nature of the magnetic and paramagnetic states in iron pnictides and iron chalcogenides, Nat. Mater. **10**, 932 (2011).

[12] Z. P. Yin, K. Haule, and G. Kotliar, Spin dynamics and orbital-antiphase pairing symmetry in iron-based superconductors, Nat. Phys. **10**, 845 (2014).

[13] N. Hao and J. Hu, Topological quantum states of matter in iron-based superconductors: From concept to material realization, Natl. Sci. Rev. **6**, 213 (2019).

[14] X. Ma, G. Wang, R. Liu, T. Yu, Y. Peng, P. Zheng, and Z. Yin, Correlation-corrected band topology and topological surface states in iron-based superconductors, Phys. Rev. B **106**, 115114 (2022).

[15] G. Xu, B. Lian, P. Tang, X.-L. Qi, and S.-C. Zhang, Topological superconductivity on the surface of Fe-based superconductors, Phys. Rev. Lett. **117**, 047001 (2016).

[16] X. Wu, S. Qin, Y. Liang, H. Fan, and J. Hu, Topological characters in Fe(Te$_{1-x}$Se$_x$) thin films, Phys. Rev. B **93**, 115129 (2016).

[17] N. Hao and J. Hu, Topological phases in the single-layer FeSe, Phys. Rev. X **4**, 031053 (2014).

[18] S. Zhu, L. Kong, L. Cao, H. Chen, M. Papaj, S. Du, Y. Xing, W. Liu, D. Wang, C. Shen, F. Yang, J. Schneeloch, R. Zhong, G. Gu, L. Fu, Y.-Y. Zhang, H. Ding, and H.-J. Gao, Nearly quantized conductance plateau of vortex zero mode in an iron-based superconductor, Science **367**, 189 (2020).

[19] X. Shi, Z.-Q. Han, P. Richard, X.-X. Wu, X.-L. Peng, T. Qian, S.-C. Wang, J.-P. Hu, Y.-J. Sun, and H. Ding, FeTe$_{1-x}$Se$_x$ monolayer films: Towards the realization of high-temperature connate topological superconductivity, Sci. Bull. **62**, 503 (2017).

[20] L. Kong, S. Zhu, M. Papaj, H. Chen, L. Cao, H. Isobe, Y. Xing, W. Liu, D. Wang, P. Fan, Y. Sun, S. Du, J. Schneeloch, R. Zhong, G. Gu, L. Fu, H.-J. Gao, and H. Ding, Half-integer level shift of vortex bound states in an iron-based superconductor, Nat. Phys. **15**, 1181 (2019).

[21] Z. Wang, P. Zhang, G. Xu, L. K. Zeng, H. Miao, X. Xu, T. Qian, H. Weng, P. Richard, A. V. Fedorov, H. Ding, X. Dai, and Z. Fang, Topological nature of the FeSe$_{0.5}$Te$_{0.5}$ superconductor, Phys. Rev. B **92**, 115119 (2015).

[22] Q. Liu, C. Chen, T. Zhang, R. Peng, Y.-J. Yan, C.-H.-P. Wen, X. Lou, Y.-L. Huang, J.-P. Tian, X.-L. Dong, G.-W. Wang, W.-C. Bao, Q.-H. Wang, Z.-P. Yin, Z.-X. Zhao, and D.-L. Feng, Robust and clean Majorana zero mode in the vortex core of high-temperature superconductor (Li$_{0.84}$Fe$_{0.16}$)OHFeSe, Phys. Rev. X **8**, 041056 (2018).

[23] W. Liu, L. Cao, S. Zhu, L. Kong, G. Wang, M. Papaj, P. Zhang, Y.-B. Liu, H. Chen, G. Li, F. Yang, T. Kondo, S. Du, G.-H. Cao, S. Shin, L. Fu, Z. Yin, H.-J. Gao, and H. Ding, A new Majorana platform in an Fe-As bilayer superconductor, Nat. Commun. **11**, 5688 (2020).

[24] P. Zhang, K. Yaji, T. Hashimoto, Y. Ota, T. Kondo, K. Okazaki, Z. Wang, J. Wen, G. D. Gu, H. Ding, and S. Shin, Observation of topological superconductivity on the surface of an iron-based superconductor, Science **360**, 182 (2018).

[25] P. Zhang, Z. Wang, X. Wu, K. Yaji, Y. Ishida, Y. Kohama, G. Dai, Y. Sun, C. Bareille, K. Kuroda, T. Kondo, K. Okazaki, K. Kindo, X. Wang, C. Jin, J. Hu, R. Thomale, K. Sumida, S. Wu, K. Miyamoto *et al.*, Multiple topological states in iron-based superconductors, Nat. Phys. **15**, 41 (2019).

[26] L. Fu and C. L. Kane, Superconducting proximity effect and MajoranaFermions at the surface of a topological insulator, Phys. Rev. Lett. **100**, 096407 (2008).

[27] D. Wang, L. Kong, P. Fan, H. Chen, S. Zhu, W. Liu, L. Cao, Y. Sun, S. Du, J. Schneeloch, R. Zhong, G. Gu, L. Fu, H. Ding, and H.-J. Gao, Evidence for Majorana bound states in an iron-based superconductor, Science **362**, 333 (2018).

[28] S. A. Yang, H. Pan, and F. Zhang, Dirac and Weyl superconductors in three dimensions, Phys. Rev. Lett. **113**, 046401 (2014).

[29] T. Hashimoto, S. Kobayashi, Y. Tanaka, and M. Sato, Superconductivity in doped Dirac semimetals, Phys. Rev. B **94**, 014510 (2016).

[30] S. Kobayashi and M. Sato, Topological superconductivity in Dirac semimetals, Phys. Rev. Lett. **115**, 187001 (2015).

[31] A. Iyo, S. Ishida, H. Fujihisa, Y. Gotoh, I. Hase, Y. Yoshida, H. Eisaki, and K. Kawashima, Superconductivity in uncollapsed tetragonal LaFe$_2$As$_2$, J. Phys. Chem. Lett. **10**, 1018 (2019).

[32] T. Gorni, D. Florez-Ablan, and L. de' Medici, Rationalizing doping and electronic correlations in LaFe$_2$As$_2$, Phys. Rev. B **107**, 125166 (2023).

[33] I. Pallecchi, E. Stellino, P. Postorino, A. Iyo, H. Ogino, M. Affronte, and M. Putti, Experimental investigation of electronic interactions in collapsed and uncollapsed LaFe$_2$As$_2$ phases, Phys. Rev. B **108**, 014512 (2023).

[34] J. Zhao, Y. Wang, X. Feng, and S. A. Yang, Electronic correlations and absence of superconductivity in the collapsed phase of LaFe$_2$As$_2$, Phys. Rev. B **103**, 125125 (2021).

[35] H. Usui and K. Kuroki, Hidden robust presence of a hole Fermi surface in a heavily electron-doped iron-based superconductor LaFe$_2$As$_2$, Phys. Rev. Res. **1**, 033025 (2019).

[36] I. I. Mazin, M. Shimizu, N. Takemori, and H. O. Jeschke, Novel Fe-based superconductor LaFe$_2$As$_2$ in comparison with traditional pnictides, Phys. Rev. Lett. **123**, 267001 (2019).

[37] S. Acharya, D. Pashov, F. Jamet, and M. van Schilfgaarde, Controlling T$_c$ through band structure and correlation engineering in collapsed and uncollapsed phases of iron arsenides, Phys. Rev. Lett. **124**, 237001 (2020).

[38] D. Mou, T. Kong, W. R. Meier, F. Lochner, L.-L. Wang, Q. Lin, Y. Wu, S. L. Bud'ko, I. Eremin, D. D. Johnson, P. C. Canfield, and A. Kaminski, Enhancement of the superconducting gap by nesting in CaKFe$_4$As$_4$: A new high temperature superconductor, Phys. Rev. Lett. **117**, 277001 (2016).

[39] J. Cui, Q.-P. Ding, W. R. Meier, A. E. Böhmer, T. Kong, V. Borisov, Y. Lee, S. L. Bud'ko, R. Valentí, P. C. Canfield, and Y. Furukawa, Magnetic fluctuations and superconducting properties of CaKFe$_4$As$_4$ studied by ^{75}As NMR, Phys. Rev. B **96**, 104512 (2017).

[40] T. Xie, Y. Wei, D. Gong, T. Fennell, U. Stuhr, R. Kajimoto, K. Ikeuchi, S. Li, J. Hu, and H. Luo, Odd and even modes of neutron spin resonance in the bilayer iron-based superconductor CaKFe$_4$As$_4$, Phys. Rev. Lett. **120**, 267003 (2018).

[41] T. K. Kim, K. S. Pervakov, D. V. Evtushinsky, S. W. Jung, G. Poelchen, K. Kummer, V. A. Vlasenko, A. V. Sadakov, A. S. Usoltsev, V. M. Pudalov, D. Roditchev, V. S. Stolyarov, D. V. Vyalikh, V. Borisov, R. Valentí, A. Ernst, S. V. Eremeev, and E. V. Chulkov, Electronic structure and coexistence of superconductivity with magnetism in RbEuFe$_4$As$_4$, Phys. Rev. B **103**, 174517 (2021).

[42] F. Lochner, F. Ahn, T. Hickel, and I. Eremin, Electronic properties, low-energy Hamiltonian, and superconducting instabilities in CaKFe$_4$As$_4$, Phys. Rev. B **96**, 094521 (2017).

[43] A. Iyo, K. Kawashima, T. Kinjo, T. Nishio, S. Ishida, H. Fujihisa, Y. Gotoh, K. Kihou, H. Eisaki, and Y. Yoshida, New-structure-type Fe-based superconductors: CaAFe$_4$As$_4$ (A = K, Rb, Cs) and SrAFe$_4$As$_4$ (A = Rb, Cs), J. Am. Chem. Soc. **138**, 3410 (2016).

[44] W. R. Meier, Q.-P. Ding, A. Kreyssig, S. L. Bud'ko, A. Sapkota, K. Kothapalli, V. Borisov, R. Valentí, C. D. Batista, P. P. Orth, R. M. Fernandes, A. I. Goldman, Y. Furukawa, A. E. Böhmer, and P. C. Canfield, Hedgehog spin-vortex crystal stabilized in a hole-doped iron-based superconductor, npj Quantum Mater. **3**, 5 (2018).

[45] C. Xu, Q. Chen, and C. Cao, Unique crystal field splitting and multiband RKKY interactions in Ni-doped EuRbFe$_4$As$_4$, Commun. Phys. **2**, 16 (2019).

[46] N. Heinsdorf, M. H. Christensen, M. Iraola, S.-S. Zhang, F. Yang, T. Birol, C. D. Batista, R. Valentí, and R. M. Fernandes, Prediction of double-Weyl points in the iron-based superconductor CaKFe$_4$As$_4$, Phys. Rev. B **104**, 075101 (2021).

[47] See Supplemental Material at http://link.aps.org/supplemental/10.1103/PhysRevB.109.L241106 for computational methods, the calculations of strong topological index ν_0 in UT-LaFe$_2$As$_2$, the DFT+DMFT band structure without spin-orbit coupling (SOC) and topological property in the DFT case of UT-LaFe$_2$As$_2$, the band inversions of UT-LaFe$_2$As$_2$ in the DFT and DFT+DMFT case, electronic correlation in UT,CT-LaFe$_2$As$_2$, design of LaBaFe$_4$As$_4$, the DFT band structures of LaBaFe$_4$As$_4$, the DFT+DMFT Fermi surfaces of LaBaFe$_4$As$_4$, surface states on different terminations of LaBaFe$_4$As$_4$, the DFT and DFT+DMFT band inversion along M-A of LaBaFe$_4$As$_4$, the calculation of strong (weak) topological index ν_0 (($\nu_1\nu_2\nu_3$)) and high-order topological index Z_8 of LaBaFe$_4$As$_4$ in DFT+DMFT case, the clarification of topological surface states in LaBaFe$_4$As$_4$, modulation of the SOC gap in LaBaFe$_4$As$_4$, Weyl points and magnetism in LaBaFe$_4$As$_4$.

[48] K. Haule, C.-H. Yee, and K. Kim, Dynamical mean-field theory within the full-potential methods: Electronic structure of CeIrIn$_5$, CeCoIn$_5$, and CeRhIn$_5$, Phys. Rev. B **81**, 195107 (2010).

[49] G. Kotliar, S. Y. Savrasov, K. Haule, V. S. Oudovenko, O. Parcollet, and C. A. Marianetti, Electronic structure calculations with dynamical mean-field theory, Rev. Mod. Phys. **78**, 865 (2006).

[50] P. Blaha, K. Schwarz, G. K. Madsen, D. Kvasnicka, and J. Luitz, *WIEN2K, An Augmented Plane Wave + Local Orbitals Program for Calculating Crystal Properties* (Karlheinz Schwarz, Vienna University of Technology, Austria, 2001).

[51] K. Haule, Exact double counting in combining the dynamical mean field theory and the density functional theory, Phys. Rev. Lett. **115**, 196403 (2015).

[52] K. Haule, Quantum monte carlo impurity solver for cluster dynamical mean-field theory and electronic structure calculations with adjustable cluster base, Phys. Rev. B **75**, 155113 (2007).

[53] P. Werner, A. Comanac, L. de' Medici, M. Troyer, and A. J. Millis, Continuous-time solver for quantum impurity models, Phys. Rev. Lett. **97**, 076405 (2006).

[54] G. Pizzi, V. Vitale, R. Arita, S. Blügel, F. Freimuth, G. Géranton, M. Gibertini, D. Gresch, C. Johnson, T. Koretsune, J. Ibañez-Azpiroz, H. Lee, J.-M. Lihm, D. Marchand, A. Marrazzo, Y. Mokrousov, J. I. Mustafa, Y. Nohara, Y. Nomura, L. Paulatto *et al.*, Wannier90 as a community code: new features and applications, J. Phys.: Condens. Matter **32**, 165902 (2020).

[55] Q. Wu, S. Zhang, H.-F. Song, M. Troyer, and A. A. Soluyanov, Wanniertools: An open-source software package for novel topological materials, Comput. Phys. Commun. **224**, 405 (2018).

[56] G. Kresse and J. Furthmüller, Efficiency of ab-initio total energy calculations for metals and semiconductors using a plane-wave basis set, Comput. Mater. Sci. **6**, 15 (1996).

[57] N. Marzari, A. A. Mostofi, J. R. Yates, I. Souza, and D. Vanderbilt, Maximally localized Wannier functions: Theory and applications, Rev. Mod. Phys. **84**, 1419 (2012).

[58] P. E. Blöchl, Projector augmented-wave method, Phys. Rev. B **50**, 17953 (1994).

[59] J. P. Perdew, K. Burke, and M. Ernzerhof, Generalized gradient approximation made simple, Phys. Rev. Lett. **77**, 3865 (1996).

[60] K. Haule and T. Birol, Free energy from stationary implementation of the DFT + DMFT functional, Phys. Rev. Lett. **115**, 256402 (2015).

[61] K. Haule and G. L. Pascut, Forces for structural optimizations in correlated materials within a DFT + embedded DMFT functional approach, Phys. Rev. B **94**, 195146 (2016).

[62] A. Togo and I. Tanaka, First principles phonon calculations in materials science, Scr. Mater. **108**, 1 (2015).

[63] L. Fu and C. L. Kane, Topological insulators with inversion symmetry, Phys. Rev. B **76**, 045302 (2007).

[64] G. Khanal and K. Haule, Correlation driven phonon anomalies in bulk FeSe, Phys. Rev. B **102**, 241108(R) (2020).

[65] P. J. Hirschfeld, M. M. Korshunov, and I. I. Mazin, Gap symmetry and structure of Fe-based superconductors, Rep. Prog. Phys. **74**, 124508 (2011).

[66] I. I. Mazin, Superconductivity gets an iron boost, Nature (London) **464**, 183 (2010).

[67] L. Fu, C. L. Kane, and E. J. Mele, Topological insulators in three dimensions, Phys. Rev. Lett. **98**, 106803 (2007).

[68] Z. Ringel, Y. E. Kraus, and A. Stern, Strong side of weak topological insulators, Phys. Rev. B **86**, 045102 (2012).

[69] E. Khalaf, H. C. Po, A. Vishwanath, and H. Watanabe, Symmetry indicators and anomalous surface states of topological crystalline insulators, Phys. Rev. X **8**, 031070 (2018).

[70] Z. Song, Z. Fang, and C. Fang, $(d − 2)$-dimensional edge states of rotation symmetry protected topological states, Phys. Rev. Lett. **119**, 246402 (2017).

[71] C. Fang and L. Fu, New classes of topological crystalline insulators having surface rotation anomaly, Sci. Adv. **5**, eaat2374 (2019).

[72] C. Fang, M. J. Gilbert, X. Dai, and B. A. Bernevig, Multi-Weyl topological semimetals stabilized by point group symmetry, Phys. Rev. Lett. **108**, 266802 (2012).

[73] L. Ortenzi, I. I. Mazin, P. Blaha, and L. Boeri, Accounting for spin fluctuations beyond local spin density approximation in the density functional theory, Phys. Rev. B **86**, 064437 (2012).

[74] J. Xiao and B. Yan, First-principles calculations for topological quantum materials, Nat. Rev. Phys. **3**, 283 (2021).

[75] Z. Wang, Y. Sun, X.-Q. Chen, C. Franchini, G. Xu, H. Weng, X. Dai, and Z. Fang, Dirac semimetal and topological phase transitions in A$_3$Bi (A = Na, K, Rb), Phys. Rev. B **85**, 195320 (2012).

[76] C. Le, X. Wu, S. Qin, Y. Li, R. Thomale, F.-C. Zhang, and J. Hu, Dirac semimetal in β-CuI without surface Fermi arcs, Proc. Natl. Acad. Sci. USA **115**, 8311 (2018).

[77] S. Jiang, H. Xing, G. Xuan, C. Wang, Z. Ren, C. Feng, J. Dai, Z. Xu, and G. Cao, Superconductivity up to 30 K in the vicinity of the quantum critical point in BaFe$_2$(As$_{1−x}$P$_x$)$_2$, J. Phys.: Condens. Matter **21**, 382203 (2009).

[78] H. C. Po, A. Vishwanath, and H. Watanabe, Symmetry-based indicators of band topology in the 230 space groups, Nat. Commun. **8**, 50 (2017).